SPEKTRA: Jurnal Fisika dan Aplikasinya
Volume 11, Issue 1, April 2026
Homepage: doi.org/10.21009/SPEKTRA

DOI: doi.org/10.21009/SPEKTRA.111.06

Optical and Photoluminescence Properties of Eu^{3+} ion doped Gadolinium Silica-phosphate Glasses

Elyzabeth Simanullang[1], Winsyahputra Ritonga[1], Juniastel Rajagukguk[1,*], Donna Helen Rajagukguk [1], Chayani Sarumaha[2], Jakrapong Kaewkhao[3,4]

[1]*Department of Physics, Faculty of Mathematics and Natural Sciences, Universitas Negeri Medan, Medan 20221, Indonesia*
[2]*Faculty of Science and Technology, Muban Chombueng Rajabhat University, Ratchaburi 70150, Thailand*
[3]*Center of Excellence in Glass Technology and Materials Science (CEGM), Nakhon Pathom Rajabhat University, Nakhon Pathom 73000, Thailand*
[4]*Physics Program, Faculty of Science and Technology, Nakhon Pathom Rajabhat University, Nakhon Pathom, Thailand*

*Corresponding Author Email: juniastel@unimed.ac.id

Received: 2 March 2026
Revised: 10 April 2026
Accepted: 13 April 2026
Online: 30 April 2026
Published: 30 April 2026

SPEKTRA: Jurnal Fisika dan Aplikasinya
p-ISSN: 2541-3384
e-ISSN: 2541-3392

CC BY

ABSTRACT

Eu^{3+}-doped gadolinium silica-phosphate glasses with compositions of $57P_2O_5$–$15QS$–$15CaO$–$5BaO$–$5Gd_2O_5$–$3Eu_2O_3$ (PCBGO) and $57P_2O_5$–$15QS$–$15CaO$–$5BaO$–$5GdF_3$–$3Eu_2O_3$ (PCBGF) were successfully synthesized using the melt-quenching technique employing natural quartz sand from Huta Ginjang, North Sumatra, Indonesia, as a silica source. The structural, optical, and photoluminescence properties of the prepared glasses were systematically investigated through X-ray diffraction (XRD), Fourier Transform Infrared (FTIR), UV-Vis-NIR absorption spectroscopy, photoluminescence spectroscopy, Judd-Ofelt (J-O) analysis, lifetime measurements and CIE chromaticity analysis. XRD results confirmed the amorphous characteristics of both glasses, while FTIR spectra revealed the formation of silica-phosphate structural networks. The incorporation of GdF_3 significantly improved glass transparency and reduced hydroxyl-related defects compared with Gd_2O_3 containing glass. Absorption spectra exhibited characteristic Eu^{3+} transitions at 392, 464, 531, 2085, and 2210 nm. Judd-Ofelt analysis demonstrated that PCBGF glass possessed a higher Ω_2 parameter, indicating increased local asymmetry and stronger covalent interaction around Eu^{3+} ions. Excitation and emission spectra revealed intense red luminescence dominated by the hypersensitive $^5D_0 \rightarrow {}^7F_2$ transition centered at 613 nm. The PCBGF glass exhibited superior photoluminescence intensity, larger stimulated emission cross-section, and enhanced radiative efficiency due to the lower phonon energy of the fluoride-containing host matrix. Lifetime analysis

showed experimental decay times of 1.823 and 1.029 ms for PCBGO and PCBGF, respectively, indicating enhanced radiative transition probability in PCBGF glass. The chromaticity coordinates for both glasses were determined to be (0.571, 0.302), located within the red region of the CIE 1931 diagram. These findings demonstrate that fluoride incorporation effectively enhances the optical and luminescence properties of Eu^{3+}-doped silica-phosphate glasses, making PCBGF a promising material for red phosphors, optical amplifiers, solid-state lasers, and advanced photonic applications.

Keywords: Eu^{3+} ions, gadolinium, silica-phosphate glass, photoluminescence, Judd-Ofelt

INTRODUCTION

Phosphate-based glasses have attracted considerable attention in modern photonic technology owing to their excellent rare-earth ion solubility, high transparency, low melting temperature, and tunable optical characteristics. These advantages make phosphate glasses promising candidates for solid-state lasers, optical amplifiers, scintillators, phosphors, radiation detectors, and photoluminescent devices [1, 2]. Compared with conventional silicate glasses, phosphate glasses possess lower glass transition and melting temperatures, enabling easier fabrication and better incorporation of rare-earth ions without severe crystallization. Furthermore, the relatively open network structure of phosphate glasses facilitates efficient luminescence transitions of rare-earth ions, thereby enhancing their applicability in photonic and optoelectronic systems [3]. Despite these advantages, pure phosphate glass generally exhibits poor chemical durability and hygroscopic behavior, which can limit its long-term stability and optical performance. Therefore, suitable modification of the phosphate network is essential to improve the structural rigidity, thermal stability, and resistance to moisture attack [4].

Incorporation of alkaline earth oxides such as CaO and BaO into phosphate glass systems has been widely recognized as an effective strategy for improving glass stability and optical performance. CaO acts as a network modifier that strengthens the phosphate framework through the formation of P-O-Ca bonds, resulting in enhanced mechanical strength and chemical durability. Meanwhile, BaO contributes to increased density, refractive index, and radiation absorption capability due to its relatively high molecular weight [5, 6]. The simultaneous presence of CaO and BaO is also beneficial for reducing non-radiative relaxation processes and improving the luminescence efficiency of rare-earth ions embedded in the glass matrix [7]. In addition, the introduction of silica compounds into phosphate-based glasses can further improve the rigidity of the glass network and suppress hygroscopic effects. However, investigations concerning the utilization of natural quartz sand as a silica precursor for rare-earth-doped photonic glasses remain very limited. This issue is scientifically important because natural quartz resources offer low-cost, environmentally sustainable, and locally abundant alternatives for advanced glass fabrication [8]. Furthermore, from a fundamental physics standpoint, the unique chemical profile and naturally occurring trace elements in

natural sand can induce minor structural distortions within the glass network. These changes in local symmetry around the Eu^{3+} coordination sites directly influence the crystal field and radiative transition probabilities, thereby altering the photoluminescence performance

The present study employs quartz sand (QS) obtained from Huta Ginjang Village, North Tapanuli, North Sumatra, Indonesia, as a silica source for the fabrication of gadolinium silica-phosphate glasses. Huta Ginjang quartz sand is particularly attractive due to its high silica content and excellent transparency potential, originating from volcanic and highland geological formations [9]. The incorporation of quartz sand into phosphate glass matrices is expected to produce a more compact and stable glass network while simultaneously maintaining favorable optical transparency. From a technological perspective, the use of naturally derived silica sources also supports the development of sustainable photonic materials and value-added utilization of local mineral resources. Therefore, this work not only contributes to the advancement of rare-earth-doped optical glasses but also introduces an alternative approach for developing functional photonic materials based on Indonesian natural resources.

Rare-earth ions are widely used as luminescence centers because of their unique electronic configurations involving partially filled 4f orbitals, which generate sharp emission bands and long excited-state lifetimes. Among various rare-earth ions, Eu^{3+} is one of the most extensively investigated luminescent activators because of its well-defined energy level structure and intense red emission originating from the $^5D_0 \rightarrow {}^7F_J$ transitions. The hypersensitive $^5D_0 \rightarrow {}^7F_2$ transition is particularly sensitive to the local symmetry around Eu^{3+} ions, making Eu^{3+} an excellent spectroscopic probe for evaluating structural changes in glass hosts [3, 10]. In addition, Eu^{3+} activated glasses have significant potential applications in solid-state lighting, display technology, optical sensors, lasers, and photonic conversion devices. Consequently, understanding the optical absorption and photoluminescence behavior of Eu^{3+} ions in different glass environments is highly important for optimizing luminescent performance.

Another important aspect of this study is the comparison between oxide-based and fluoride-based gadolinium compounds, namely Gd_2O_3 and GdF_3, incorporated into the silica-phosphate glass matrix. Gd_2O_3 is commonly utilized as an oxide modifier that enhances density, structural compactness, and radiation interaction capability due to the high atomic number of gadolinium ions [11]. Moreover, gadolinium-containing glasses are attractive for scintillation and radiation detection applications because Gd^{3+} possesses a large neutron capture cross-section and favorable energy transfer characteristics. In contrast, GdF_3 plays an important role in reducing phonon energy within the glass matrix because fluoride ions exhibit lower vibrational energy compared with oxide ions [11, 12]. Lower phonon energy environments are highly advantageous for suppressing non-radiative multiphonon relaxation processes, thereby improving radiative emission efficiency and photoluminescence intensity [13]. Therefore, comparing Gd_2O_3 and GdF_3 containing glasses provides valuable insight into the influence of oxide and fluoride environments on the structural and spectroscopic properties of Eu_{3+} doped silica-phosphate glasses.

Although numerous studies have reported Eu^{3+} doped phosphate or fluorophosphate glasses, comparative investigations involving natural quartz sand derived silico-phosphate glasses

containing both Gd_2O_3 and GdF_3 remain rarely explored. The novelty of the present work lies in the fabrication and comparative investigation of Eu^{3+} doped gadolinium silica-phosphate glasses prepared using local Huta Ginjang quartz sand as a sustainable silica source, combined with different gadolinium compounds to tailor the optical and photoluminescence properties. The relationship between glass composition, local structural environment, optical absorption characteristics, and Eu^{3+} photoluminescence behavior is systematically evaluated. This study is expected to provide new insight into the development of environmentally sustainable and high-performance photonic glass materials for future applications in luminescent devices, optical amplifiers, scintillators, and advanced photonic technologies

METHOD

Glass Preparation

Eu^{3+} doped gadolinium silica-phosphate glasses were fabricated using the conventional melt-quenching technique. Two different glass compositions were prepared, namely $57P_2O_5$–15 Quartz sand–15CaO–5BaO–$5Gd_2O_3$–$3Eu_2O_3$ and $57P_2O_5$–5 Quartz sand–15CaO–5BaO–$5GdF_3$–$3Eu_2O_3$ (PCBGF). The quartz sand used as the silica source was obtained from Huta Ginjang Village, North Tapanuli, North Sumatra, Indonesia, which has a SiO_2 purity of 99% as established in previous characterization studies [9]. All starting materials possessed a purity of 99%, and each batch composition was prepared with a total weight of 20 g. Prior to the melting process, all raw materials were accurately weighed according to the designed compositions and thoroughly mixed using an agate mortar to achieve a homogeneous mixture. The mixed powders were then transferred into an alumina crucible and melted in an electric furnace at a temperature of 1200 °C until a transparent and homogeneous molten liquid was obtained. After complete melting, the molten glass was poured into a preheated stainless-steel mold and subsequently subjected to an annealing process at 500 °C for 3 h in order to relieve internal thermal stress and prevent crack formation. After annealing, the glass samples were slowly cooled to room temperature inside the furnace. Samples exhibiting good transparency, homogeneity, and crack-free surfaces were selected for further processing. The selected glasses were cut into appropriate dimensions and carefully polished to obtain smooth and optically clear surfaces suitable for characterization measurements.

Characterization Techniques

The physical appearance and transparency of the prepared glasses were initially evaluated through visual observation. Structural characterization of the glass samples was performed using X-ray diffraction (XRD) analysis to confirm the amorphous nature of the prepared glasses. In addition, Fourier Transform Infrared (FTIR) spectroscopy was employed to investigate the vibrational characteristics and structural bonding within the glass network. The optical absorption properties of the prepared glasses were analyzed using a UV-Vis-NIR Spectrophotometer (Shimadzu UV-3600) in the ultraviolet, visible, and near-infrared regions. The photoluminescence properties were investigated using a Spectrofluorophotometer (Agilent Cary Eclipse) to evaluate the excitation and emission characteristics of Eu^{3+} ions

embedded in the gadolinium silica-phosphate glass matrices. These characterization results were further used to analyze the influence of Gd_2O_3 and GdF_3 incorporation on the structural, optical, and luminescence properties of the prepared glasses.

RESULT AND DISCUSSION

Glass Appearance and Physical Properties

The prepared Eu^{3+} doped gadolinium silica-phosphate glasses exhibited good transparency and homogeneity after the melt-quenching process, indicating the successful formation of glass media without visible crystallization. FIGURE 1 presents the physical appearance of PCBGO and PCBGF glasses before and after the cutting and polishing processes. Prior to polishing, both samples exhibited translucent characteristics with slight differences in visual appearance. The PCBGO glass containing Gd_2O_3 appeared relatively more-opaque and showed a slightly yellowish-white coloration compared with the PCBGF sample. In contrast, the PCBGF glass containing GdF_3 exhibited higher transparency and a clearer appearance even before polishing. After the cutting and polishing process, both samples demonstrated significantly improved optical transparency with smooth surfaces suitable for optical characterization. Nevertheless, the PCBGF sample still exhibited better clarity than PCBGO, indicating that fluoride incorporation plays an important role in improving the optical quality of the glass matrix.

The enhanced transparency observed in PCBGF glass can be associated with the presence of fluoride ions, which are known to reduce phonon energy and suppress structural defects responsible for light scattering within the glass network [14-16]. Fluoride incorporation also decreases the concentration of non-bridging oxygen bonds and hydroxyl groups, thereby minimizing optical losses and improving the homogeneity of the glass structure. Conversely, the incorporation of Gd_2O_3 in PCBGO tends to increase structural compactness and oxygen-related bonding interactions, which may contribute to higher scattering centers and slightly reduced transparency. The observed visual differences between both glasses therefore suggest that the substitution of oxide by fluoride compounds significantly influences the local glass structure and optical behavior.

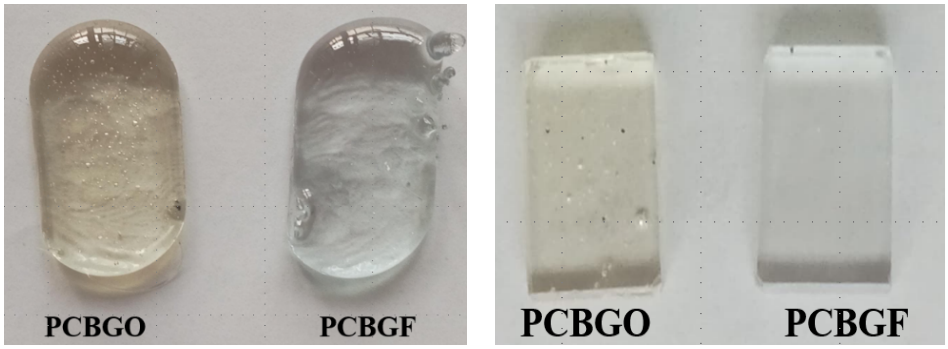

(a) (b)

FIGURE 1. Physical appearance of Eu^{3+} doped gadolinium silica-phosphate glasses: (a) before cutting and polishing and (b) after cutting and polishing for PCBGO and PCBGF samples.

The physical parameters of PCBGO and PCBGF glasses are summarized in TABLE 1. The molar weight of PCBGO glass was found to be higher than that of PCBGF glass, which is attributed to the larger molecular weight contribution of Gd_2O_3 compared with GdF_3 this result also influences several derived physical parameters, particularly density and molar volume. The density values decreased from 3.0982 g/cm^3 for PCBGO to 2.8833 g/cm^3 for PCBGF. The reduction in density after fluoride incorporation can be explained by the replacement of oxygen ions with lighter fluoride ions, which decreases the overall compactness of the glass network. Furthermore, fluoride ions generally induce a more open glass structure, resulting in increased free volume within the matrix [17]. The lower density in PCBGF consequently produced a higher molar volume (44.1396 cm^3/mol) compared with PCBGO (43.4706 cm^3/mol). Since molar volume is inversely proportional to density, the increase in molar volume indicates the expansion of the glass network and the formation of a less compact structural arrangement in the fluoride-containing glass.

The refractive index values also showed noticeable differences between the two samples, where PCBGO exhibited a higher refractive index (1.5634) than PCBGF (1.5409). This behavior is closely related to the higher density and electronic polarizability of the oxide-containing glass network [18]. In general, materials with higher density possess greater electron packing density, which contributes to stronger interaction between electromagnetic radiation and the glass medium, thereby increasing the refractive index. In addition, the higher refractive index of PCBGO indicates that the incorporation of Gd_2O_3 enhances the polarization capability of the glass network compared with fluoride incorporation. The ion concentration values were slightly higher in PCBGO glass, indicating a denser distribution of Eu^{3+} ions within the oxide-based matrix. This result is consistent with the smaller polaron radius and shorter inter-nuclear distance observed for PCBGO. Smaller inter-ionic distances generally indicate a more compact network structure and stronger local field interactions among rare-earth ions. In contrast, the larger polaron radius and inter-nuclear distance in PCBGF suggest that fluoride incorporation promotes structural expansion and reduces ionic packing density. Such structural modification is highly important in photoluminescence studies because the

TABLE 1. Physical properties of Eu3+ doped PCBGO and PCBGF silica-phosphate glasses.

Physical Properties	Samples	
	PCBGO	PCBGF
Molar weight, M (g)	134.6805	127.2678
Density, ρ (g/cm^3)	3.0982	2.8833
Molar volume, V_m (cm^3/mol)	43.4706	44.1396
Refractive index, n	1.5634	1.5409
Ion concentration, N (x10^{20} ion/cm^3)	1.3800	1.2900
Polaron radius, r_p x10^{-8}	7.7900	7.9800
Inter nuclear distance, r_i x10^{-7}	1.9300	1.9800
Dielectric constant, ε	2.4442	2.3744
Molar refractivity, R_m (cm^{-3})	14.1264	13.8681
Polarizability of oxide ions, α_m (x10^{-20} cm^3)	2.4400	2.5700
Metallization criteria, M	0.6750	0.6858
Reflection loss, R (%)	4.8306	4.5317

local environment surrounding Eu^{3+} ions strongly affects radiative transition probabilities and luminescence efficiency.

Structural Properties

XRD Analysis

The structural characteristics of the prepared Eu^{3+} doped gadolinium silica-phosphate glasses were investigated using X-ray diffraction (XRD) analysis, as presented in FIGURE 2. The diffraction patterns of both PCBGO and PCBGF glasses exhibit broad diffuse humps centered around $2\theta \approx 25°$ without the presence of sharp and well-defined crystalline diffraction peaks. This broad halo pattern confirms the amorphous nature of both prepared glasses and indicates the absence of long-range atomic ordering within the glass network [19]. The formation of an amorphous structure demonstrates that the melt-quenching technique successfully prevented crystallization during the cooling process, leading to the formation of homogeneous glass matrices. The broad diffraction band observed near 25^0 is mainly associated with the disordered arrangement of silica-phosphate structural units originating from the quartz sand (SiO_2) and phosphate network former (P_2O_5). The incorporation of modifier compounds such as CaO, BaO, Gd_2O_5, and GdF_3 contributes to the disruption of periodic atomic arrangements, thereby suppressing crystal growth and stabilizing the amorphous phase [20]. In particular, the addition of rare-earth ions such as Eu^{3+} introduces local structural distortions due to differences in ionic radius and bonding characteristics, which further hinder crystallization and promote glass formation.

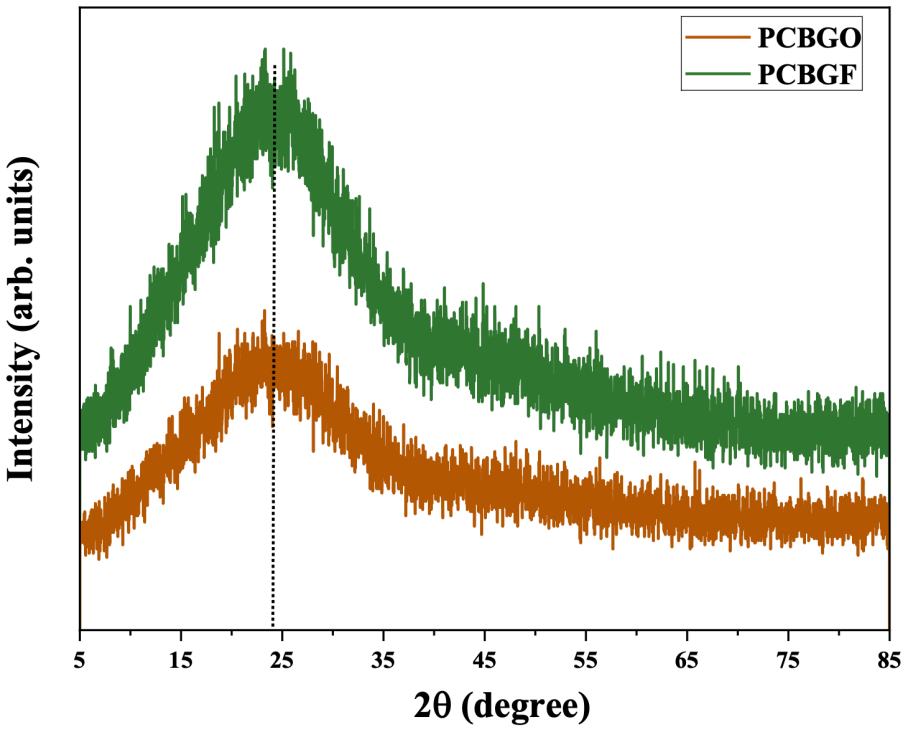

FIGURE 2. The X-ray diffraction (XRD) patterns of Eu^{3+} doped PCBGO and PCBGF silica-phosphate glasses

A slight difference in the intensity and broadness of the amorphous hump can also be observed between PCBGO and PCBGF glasses. The PCBGF sample exhibits relatively higher intensity and a slightly broader diffuse peak compared with PCBGO, suggesting that fluoride incorporation modifies the short-range structural arrangement of the glass network. Fluoride ions are known to reduce bond connectivity and decrease phonon energy within the glass matrix, leading to a more open and less rigid structure. This structural modification is consistent with the previously observed increase in molar volume and improved optical transparency of PCBGF glass [21, 22]. In contrast, the oxide-based PCBGO glass tends to form a denser and more compact structural network due to stronger oxygen-related bonding interactions.

FTIR Analysis

Further structural investigation was carried out using Fourier Transform Infrared (FTIR) spectroscopy to identify the vibrational characteristics and bonding structure of the prepared glasses. The FTIR spectra of PCBGO and PCBGF glasses in the range of 400-4000 cm^{-1} are shown in FIGURE 3, while the corresponding band assignments are summarized in TABLE 2. The observed absorption bands confirm the formation of a silica-phosphate glass network and provide important information regarding the influence of Gd_2O_3 and GdF_3 incorporation on the local structural environment.

The absorption band located in the range of 400-500 cm^{-1} is attributed to deformation vibrations of phosphate groups within the glass matrix [8]. This band is commonly associated with bending vibrations involving O-P-O linkages and indicates the successful formation of

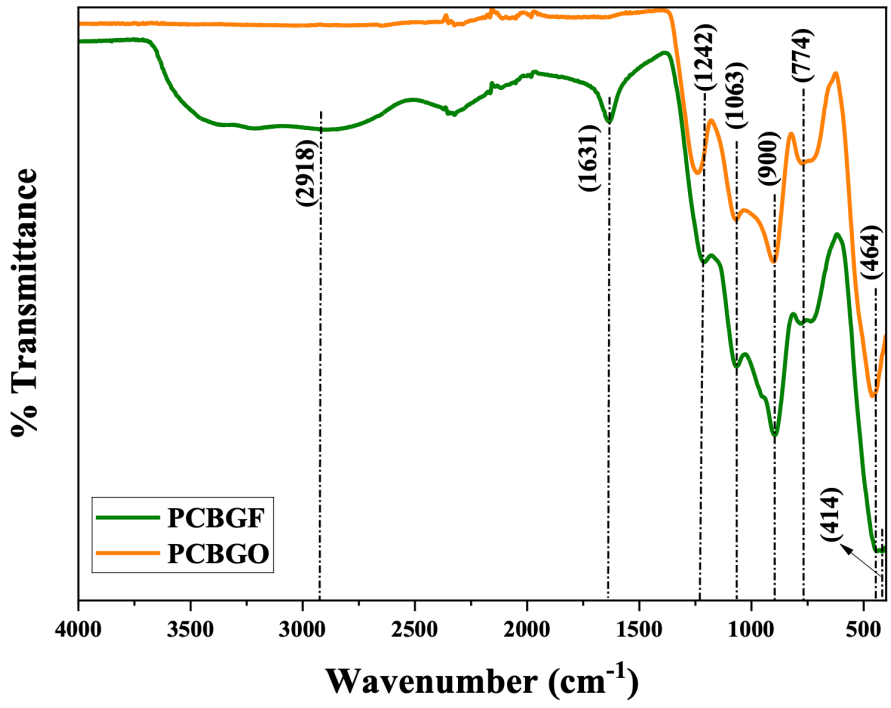

FIGURE 3. The FTIR (Fourier Transform Infrared) patterns of Eu3+ doped PCBGO and PCBGF silica-phosphate glasses

phosphate structural units in the prepared glasses. The presence of this vibrational mode suggests that phosphate compounds play an essential role as the primary glass-forming network in both PCBGO and PCBGF samples.

An absorption band observed around 774 cm^{-1} corresponds to the symmetric stretching vibration mode associated with oxygen atom movement relative to the molecular framework [23]. This vibration reflects the structural connectivity of the glass network and indicates interactions between phosphate and silica structural units. The appearance of this band also confirms that the incorporation of modifier ions does not destroy the fundamental framework structure of the silica-phosphate network.

The absorption region around 893-900 cm^{-1} is assigned to Si-O-Si and Si-O vibrational modes originating from the silica matrix derived from Huta Ginjang quartz sand [24]. The existence of this characteristic silica vibration demonstrates that the quartz sand successfully contributed to the formation of the glass network structure. Moreover, the persistence of this vibrational band after Eu^{3+} incorporation indicates that the silica framework remains structurally stable despite the addition of rare-earth ions and gadolinium compounds. This structural stability is highly important for maintaining favorable optical transparency and mechanical properties.

The weak absorption band appearing in the range of 1200-1400 cm^{-1} is attributed to the stretching vibration of P=O bonds [8]. This vibrational feature is characteristic of phosphate glass systems and is related to the presence of terminal oxygen atoms within phosphate tetrahedral units. Variations in the intensity of this band may indicate changes in the degree of phosphate network polymerization due to the incorporation of modifier ions such as Ca^{2+}, Ba^{2+}, Gd^{3+} and Eu^{3+}. The relatively broader band observed in PCBGF suggests that fluoride incorporation influences the local bonding environment and promotes structural depolymerization within the glass network.

Another significant absorption band appears around 1600-1650 cm^{-1} as shown in TABLE 2, corresponding to hydrogen bonding involving non-bridging oxygen atoms associated with P-O-H structural units [8]. This band is generally related to absorbed water molecules and hydroxyl groups within the glass matrix. Hydroxyl groups are known to influence luminescence behavior because they can act as non-radiative relaxation centers that reduce photoluminescence efficiency. Interestingly, the intensity of this band is relatively weaker in

TABLE 2. Physical properties of Eu3+ doped PCBGO and PCBGF silica-phosphate glasses.

Range (cm^{-1})	Band assignments	References
2800-3000	O-H stretching vibration	[8]
1600-1650	hydrogen bonding with non-bridging oxygen atoms, characteristic of P–O–H structural units	[8]
1200-1400	stretching modes P=O	[8]
893-900	Si-O-Si or Si-O vibration (silica matrix)	[24]
774	The symmetric stretching mode is characterized by the vertical movement of oxygen atoms	[23]
400-500	The deformation vibrations in the phosphate groups	[8]

PCBGF glass, indicating that fluoride incorporation may reduce hydroxyl concentration within the glass structure. This phenomenon is beneficial for optical applications because lower OH^- content can suppress multiphonon relaxation processes and enhance radiative emission efficiency. In the high wavenumber region around 2800-3000 cm^{-1}, a broad absorption band associated with O-H stretching vibrations is observed [8]. This band is attributed to the absorption of atmospheric moisture by the glass samples. The reduced intensity of this broadband in the fluoride-containing PCBGF sample further confirms that fluoride incorporation contributes to lowering hydroxyl-related defects and improving structural stability against moisture absorption. Such behavior is particularly advantageous for photonic materials because excessive hydroxyl content can significantly deteriorate optical transmission and luminescence performance.

Absorption Spectra and J-O Analysis

The optical absorption spectra of Eu^{3+} doped PCBGO and PCBGF glasses recorded in the UV-Vis-NIR regions are presented in FIGURE 4. Several characteristic absorption bands corresponding to intra-configurational 4f-4f transitions of Eu^{3+} ions can be clearly observed. The identified transitions are assigned to the transitions from the ground states $^7F_0$ and $^7F_1$ to the excited states $^5L_6$, $^5D_2$, $^5D_2$, and $^7F_6$, located at approximately 392, 464, 531, 2085, and 2210 nm, respectively. These absorption bands are associated with the electronic transitions of Eu^{3+} ions embedded within the silica-phosphate glass network and confirm the successful incorporation of Eu^{3+} ions into both glass matrices. The sharp and well-defined absorption peaks are characteristic of rare-earth ions due to the shielding effect of outer $5s^2$and $5p^6$ orbitals

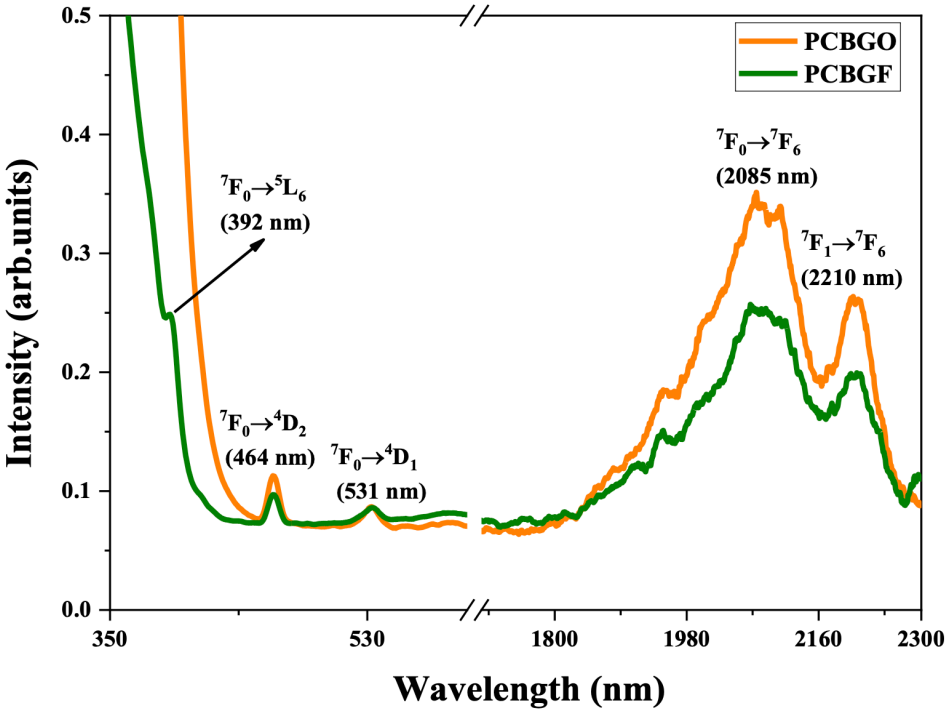

FIGURE 4. The UV-Vis-NIR absorption spectra of Eu^{3+} doped PCBGO and PCBGF silica-phosphate glasses

surrounding the partially filled 4f orbitals, which minimizes interactions with the surrounding glass environment [25].

Among the observed transitions, the absorption band centered around 392 nm corresponding to the $^7F_0 \rightarrow {}^5L_6$ transition exhibited relatively strong intensity in the visible region. This transition is commonly used as an effective excitation wavelength for Eu^{3+} activated luminescent materials because it possesses high absorption probability and efficient energy transfer characteristics [26]. In addition, strong absorption bands observed in the near-infrared region at approximately 2085 and 2210 nm correspond to the $^7F_0 \rightarrow {}^7F_6$ and $^7F_1 \rightarrow {}^7F_6$ transitions, respectively. The presence of these NIR absorption bands indicates that the prepared glasses possess potential for optical applications operating in the infrared region, including optical amplifiers and photonic conversion systems.

A comparison between both glass systems reveals that PCBGO glass exhibits slightly higher absorption intensity than PCBGF for most observed transitions. This behavior is closely related to the higher density and refractive index of PCBGO glass, which enhance the interaction between electromagnetic radiation and Eu^{3+} ions within the glass network [25]. The stronger absorption intensity in PCBGO may also suggest a relatively higher local field strength and stronger covalent interaction between Eu^{3+} ions and surrounding oxygen ligands, as inferred from the optical absorption behavior. In contrast, the incorporation of fluoride ions in PCBGF is considered to reduce local field interactions, possibly due to the lower polarizability and reduced phonon energy of fluoride environments. It should be noted that these interpretations are based on indirect optical evidence; direct structural probes such as EXAFS or NMR would be required to firmly confirm the local coordination environment and atomic arrangement, and are proposed as a direction for future work.

To further investigate the spectroscopic characteristics of Eu^{3+} ions in the prepared glasses, the experimental oscillator strengths (f_{exp}) for all observed transitions were determined from the absorption spectra. These values were subsequently used to calculate the theoretical oscillator strengths (f_{cal}) and the Judd-Ofelt (J-O) intensity parameters Ω_2, Ω_4, and Ω_6. The obtained f_{exp} and f_{cal} values, together with the root mean square deviation (δ_{rms}), are summarized in TABLE 3. The relatively low δ_{rms} values of 0.211 for PCBGO and 0.166 for PCBGF indicate good agreement between experimental and theoretical oscillator strengths,

TABLE 3. The oscillator strength of the Eu^{3+}: PCBGO and PCBGF glasses.

Transition	λ_{abs} (nm)	E_{exp} (cm^{-1})	PCBGO		PCBGF	
			f_{exp}	f_{cal}	f_{exp}	f_{cal}
$^7F_0 \rightarrow {}^5L_6$	393	25445.29	0.026	0.081	0.094	0.165
$^7F_0 \rightarrow {}^5D_2$	464	21551.72	0.116	0.035	0.153	0.039
$^7F_1 \rightarrow {}^5D_1$	533	18761.73	0.068	0.071	0.122	0.133
$^7F_0 \rightarrow {}^7F_6$	2085	4835.59	0.913	0.386	0.961	0.561
$^7F_1 \rightarrow {}^7F_6$	2210	4526.94	0.251	0.314	0.408	0.455
δ_{rms}			0.211		0.166	

confirming the applicability and reliability of the Judd-Ofelt theory for analyzing the spectroscopic behavior of Eu^{3+} ions in these glass systems.

The Judd-Ofelt intensity parameters provide important information regarding the local structural environment, bonding nature, and rigidity of the host matrix surrounding rare-earth ions. The Ω_2 parameter is highly sensitive to the asymmetry and covalency of the metal–ligand bond around Eu^{3+} ions, while Ω_4 and Ω_6 are generally associated with the rigidity, viscosity, and long-range structural properties of the glass host [27]. As presented in TABLE 4, PCBGO glass exhibits the trend $\Omega_4 > \Omega_2 > \Omega_6$ with values of $\Omega_2 = 1.349 \times 10^{-20}$ cm², $\Omega_4 = 5.105 \times 10^{-20}$ cm^2, and $\Omega_6 = 0.362 \times 10^{-20}$ cm^2. The relatively high Ω_4 value suggests that PCBGO possesses a more rigid and compact oxide-based glass network due to the presence of Gd_2O_3 and stronger oxygen coordination within the matrix. The larger Ω_4 parameter also indicates enhanced structural stability and increased viscosity of the glass host.

In contrast, PCBGF glass exhibits the trend $\Omega_2 > \Omega_4 > \Omega_6$ with $\Omega_2 = 1.528 \times 10^{-20}$ cm^2, $\Omega_4 = 1.269 \times 10^{-20}$ cm^2, and $\Omega_6 = 0.535 \times 10^{-20}$ cm^2. The higher Ω_2 value in PCBGF indicates that the local environment surrounding Eu^{3+} ions becomes more asymmetric and chemically covalent after fluoride incorporation. Fluoride ions are known to modify the local coordination environment and reduce network connectivity, leading to structural depolymerization and increased asymmetry around rare-earth ions. This result is consistent with the FTIR analysis, which revealed that PCBGF possesses a more open glass structure and lower hydroxyl concentration. The larger Ω_2 value also suggests that PCBGF glass may exhibit enhanced hypersensitive transitions and improved luminescence efficiency because Ω_2 is closely related to electric dipole transition probabilities. The spectroscopic quality factor χ (Ω_2/Ω_6) provides additional information regarding the radiative properties and optical quality of the prepared glasses. PCBGO glass exhibits a significantly higher χ value (14.10) compared with PCBGF (2.371), indicating that PCBGO possesses stronger structural rigidity and potentially better radiative stability. Meanwhile, the lower χ value in PCBGF reflects the influence of fluoride ions in producing a less rigid but optically more flexible glass network. Similar trends have also been reported in other Eu^{3+} -doped silicate and sol-gel glass systems, as presented in TABLE 4 [28, 29].

TABLE 4. The Judd-Ofelt intensity parameters (Ω_2, Ω_4, and Ω_6 $\times 10^{-20}$) and spectroscopic quality factor ($\chi = \Omega_4/\Omega_6$) of Eu^{3+} -doped PCBGO and PCBGF glasses compared with reported glass systems.

Glass	Ω_2	Ω_4	Ω_6	$\chi(\Omega_4/\Omega_6)$	Trend	Ref.
PCBGO	1.349	5.105	0.362	14.10	$\Omega_4 > \Omega_2 > \Omega_6$	Sample
PCBGF	1.528	1.269	0.535	2.371	$\Omega_2 > \Omega_4 > \Omega_6$	Sample
SiEU4	1.048	1.900	1.8709	1.0155	$\Omega_2 < \Omega_4 > \Omega_6$	[25]
Eu^{3+}/ sol-gel	2.4	1.99	0.996	1.998	$\Omega_2 > \Omega_4 > \Omega_6$	[26]

Photoluminescence Spectra

Excitation Spectra

The excitation spectra of Eu^{3+}-doped PCBGO and PCBGF glasses monitored at the emission wavelength of 613 nm are presented in FIGURE 5. Several well-defined excitation bands associated with Gd^{3+} and Eu^{3+} ions can be clearly observed in the ultraviolet and visible regions, confirming the efficient optical activity of the prepared silica-phosphate glasses. The broad excitation band centered around 225 nm is attributed to the charge transfer band (CTB) corresponding to the $O^{2-}\rightarrow Eu^{3+}$ transition. This transition originates from electron transfer between oxygen ligands and Eu^{3+} ions and is commonly observed in Eu^{3+} -activated oxide glass systems [30, 31]. The CTB intensity of PCBGF glass is significantly higher than that of PCBGO, indicating that fluoride incorporation enhances the local asymmetry and modifies the ligand field surrounding Eu^{3+} ions.

In addition to the CTB, several sharp excitation peaks associated with intra-configurational 4f-4f transitions of Eu^{3+} ions are observed at approximately 287, 298, 320, 362, 382, 394, 414, 463, 525, and 534 nm. These transitions correspond to $^7F_0 \rightarrow (^5I_6, ^5H_6)$, $^7F_0\rightarrow ^5F_4$, $^7F_0\rightarrow ^5H_4$, $^7F_0\rightarrow ^5D_4$, $^7F_0\rightarrow ^5G_4$, $^7F_0\rightarrow ^5L_6$, $^7F_1\rightarrow ^5D_3$, $^7F_1\rightarrow ^5D_2$, $^7F_0\rightarrow ^5D_0$, and $^7F_1\rightarrow ^5D_0$ transitions, respectively. Among these transitions, the most intense excitation peak appears at 394 nm, corresponding to the $^7F_0\rightarrow ^5L_6$ transition of Eu^{3+}. This transition is a partially allowed magnetic-dipole transition and is widely recognized as one of the most efficient excitation

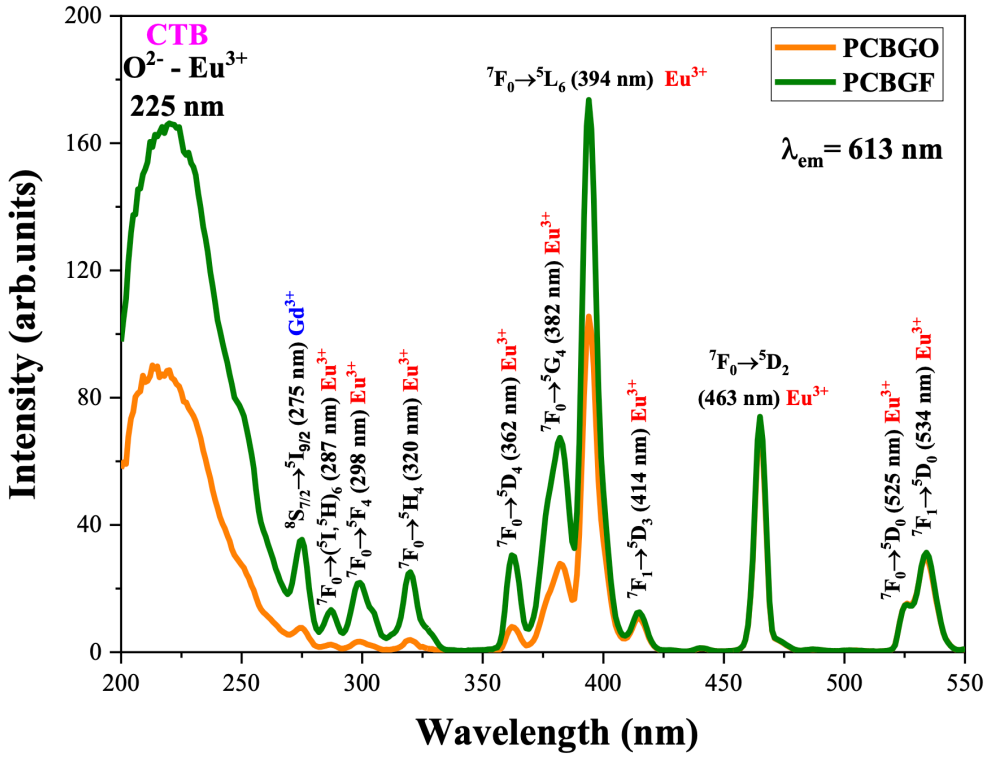

FIGURE 5. The excitation spectra of Eu^{3+} doped PCBGO and PCBGF glasses monitored at λ_{em} = 613 nm

pathways for Eu^{3+} luminescent materials because it effectively populates the excited $^5D_0$ state responsible for red emission at 613 nm [32].

Another important excitation feature observed in the range of 250-280 nm is attributed to the $^8S_{7/2} \rightarrow {}^5I_{9/2}$ transition of Gd^{3+} ions. The intensity of this Gd^{3+} related excitation band is noticeably stronger in PCBGF glass compared with PCBGO. This result suggests that the incorporation of GdF_3 promotes more efficient energy absorption and transfer processes within the glass matrix. The simultaneous presence of Gd^{3+} and Eu^{3+} excitation bands indicates the occurrence of energy transfer interactions between Gd^{3+} sensitizer ions and Eu^{3+} activator ions [33]. The absorbed energy by Gd^{3+} ions can be transferred non-radiatively to Eu^{3+} ions, thereby enhancing Eu^{3+} luminescence efficiency. The stronger excitation intensity observed in PCBGF glass can be correlated with the lower phonon energy of fluoride-containing environments. Fluoride ions reduce non-radiative multiphonon relaxation processes, resulting in improved radiative transition probabilities and enhanced excitation efficiency [30]. Furthermore, the lower hydroxyl concentration previously observed in FTIR analysis also contributes to minimizing non-radiative losses. Therefore, the excitation spectra confirm that the fluoride-containing PCBGF glass provides a more favorable optical environment for Eu^{3+} luminescence compared with the oxide-based PCBGO glass.

Emission Spectra

The emission spectra of PCBGO and PCBGF glasses under excitation wavelengths of 275 and 394 nm are shown in FIGURE 6(a) and FIGURE 6(b), respectively. Both spectra exhibit several characteristic emission bands originating from radiative transitions of Eu^{3+} ions from the excited $^5D_0$ state to the lower ^7F_J (J = 0-4) energy levels. The observed emission peaks located at approximately 578, 591, 613, 652, and 700 nm correspond to the $^5D_0 \rightarrow {}^7F_0$, $^5D_0 \rightarrow {}^7F_1$, $^5D_0 \rightarrow {}^7F_2$, $^5D_0 \rightarrow {}^7F_3$, and $^5D_0 \rightarrow {}^7F_4$ transitions, respectively [30]. The sharp and narrow emission lines are characteristic features of 4f–4f transitions in rare-earth ions, which remain relatively

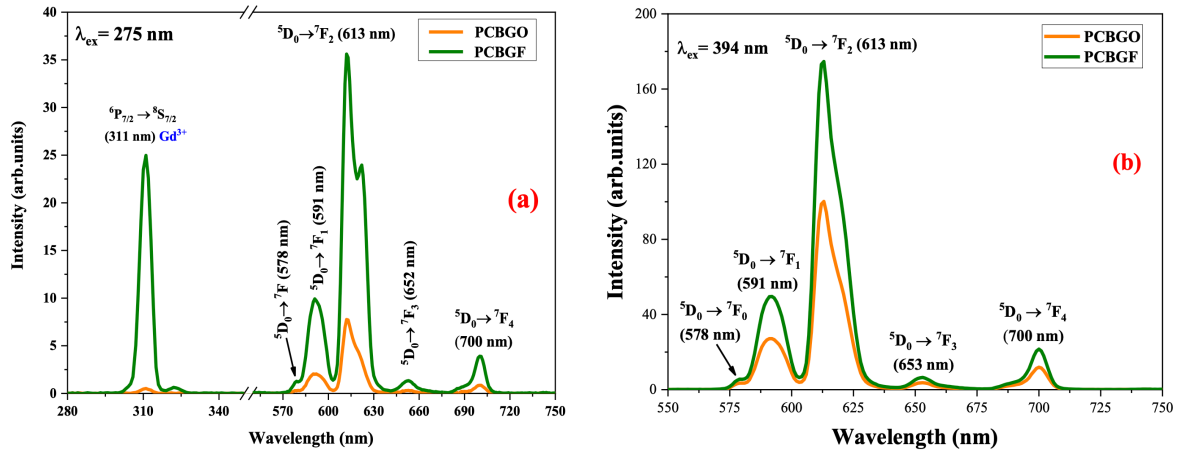

(a) (b)

FIGURE 6. Emission spectra of PCBGO and PCBGF glasses for (a) λ_{ex} = 275 nm and (b) λ_{ex} = 394 nm

unaffected by the surrounding host matrix due to shielding by outer $5s^2$ and $5p^6$ orbitals. Under excitation at 275 nm, the emission spectra reveal the presence of an additional emission band centered around 311 nm, which is attributed to the $^6P_{7/2} \rightarrow {}^8S_{7/2}$ transition of Gd^{3+} ions. The appearance of this Gd^{3+} emission band confirms the participation of Gd^{3+} ions in the excitation process and indicates the occurrence of energy transfer from Gd^{3+} to Eu^{3+} ions [34]. The gradual decrease in Gd^{3+} emission intensity accompanied by the enhancement of Eu^{3+} emission intensity strongly suggests an efficient non-radiative energy transfer mechanism between Gd^{3+} and Eu^{3+} ions through the $(^8S_{7/2} \rightarrow {}^5I_{9/2}) \rightarrow (^5D_0 \rightarrow {}^7F_J)$ pathway. Such energy transfer processes are highly beneficial for improving luminescence efficiency because Gd^{3+} ions can act as sensitizers that effectively absorb ultraviolet radiation and transfer energy to Eu^{3+} activator ions.

Among all observed transitions, the $^5D_0 \rightarrow {}^7F_2$ transition centered at 613 nm exhibits the highest emission intensity for both excitation wavelengths. This transition corresponds to an electric-dipole hypersensitive transition that strongly depends on the local symmetry surrounding Eu^{3+} ions [16, 32]. The dominance of the red emission band indicates that Eu^{3+} ions occupy non-centrosymmetric sites within the glass matrix, leading to enhanced electric-dipole transition probability. In contrast, the $^5D_0 \rightarrow {}^7F_1$ transition at 591 nm corresponds to a magnetic-dipole transition, which is less sensitive to changes in the local environment and is generally associated with centrosymmetric sites. A comparison between PCBGO and PCBGF glasses demonstrates that PCBGF exhibits significantly higher photoluminescence intensity than PCBGO under both excitation wavelengths. This enhancement can be attributed to several structural and spectroscopic factors. First, the incorporation of fluoride ions lowers the phonon energy of the host matrix, thereby suppressing non-radiative multiphonon relaxation processes. Second, the reduced hydroxyl concentration in PCBGF glass minimizes quenching centers associated with OH^- groups. Third, the higher Ω_2 value obtained from Judd-Ofelt analysis indicates greater asymmetry and covalent interaction around Eu^{3+} ions, which favors stronger electric-dipole transitions, particularly the hypersensitive $^5D_0 \rightarrow {}^7F_2$ transition.

Under direct excitation at 394 nm corresponding to the $^7F_0 \rightarrow {}^5L_6$ transition of Eu^{3+}, the photoluminescence intensity increases substantially compared with excitation at 275 nm. This behavior confirms that the 394 nm excitation wavelength provides more efficient direct excitation of Eu^{3+} ions into higher excited states, followed by rapid non-radiative relaxation to the emitting $^5D_0$ level. Nevertheless, regardless of the excitation wavelength employed, the strongest emission consistently occurs at 613 nm, indicating the dominance of red luminescence in both glass systems.

Lifetime and Radiative Properties

Lifetime

The luminescence decay curves corresponding to the $^5D_0 \rightarrow {}^7F_2$ transition of Eu^{3+} ions recorded at λ_{ex} = 394 nm and λ_{em} = 613 nm are presented in FIGURE 7. The decay profiles for both PCBGO and PCBGF glasses exhibit nearly exponential behavior, indicating that Eu^{3+} ions are relatively uniformly distributed within the glass matrix and occupy similar local environments.

The decay characteristics provide important information regarding the energy transfer processes, radiative relaxation mechanisms, and local structural dynamics surrounding Eu^{3+} ions in the prepared glasses [35].

The experimental lifetimes obtained from the decay curves are 1.823 ms for PCBGO and 1.029 ms for PCBGF. The shorter lifetime observed in PCBGF glass indicates that the relaxation process occurs more rapidly in the fluoride-containing host matrix. This behavior can be associated with increased radiative transition probability and enhanced electric-dipole transitions resulting from the more asymmetric local environment around Eu^{3+} ions, as confirmed by the larger Ω_2 parameter obtained from Judd-Ofelt analysis [33]. The increased asymmetry promotes stronger hypersensitive $^5D_0 \rightarrow {}^7F_2$ transitions, leading to more efficient radiative emission and consequently shorter luminescence lifetime.

Although PCBGF exhibits shorter experimental lifetime, its photoluminescence intensity remains significantly higher than that of PCBGO. This phenomenon suggests that the decrease in lifetime is mainly associated with enhanced radiative decay rather than increased non-radiative losses. The incorporation of GdF_3 reduces phonon energy and suppresses multi phonon relaxation processes, thereby improving luminescence efficiency despite the shorter decay time. In contrast, the longer lifetime observed in PCBGO glass may be related to slower radiative relaxation processes and stronger structural rigidity within the oxide-based glass network [36]. The discrepancy between calculated radiative lifetimes and experimental decay lifetimes further indicates the contribution of additional relaxation mechanisms within the glass matrix, including local field effects, structural inhomogeneity, and energy transfer interactions between Gd^{3+} and Eu^{3+} ions. Furthermore, hydroxyl-related defects and non-bridging oxygen groups can influence relaxation dynamics by introducing additional non-

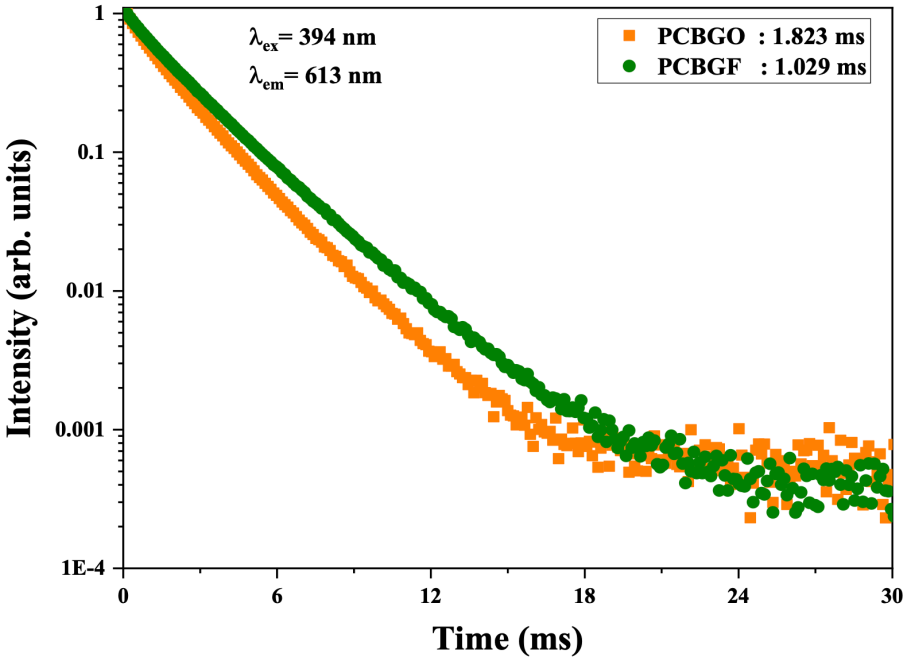

FIGURE 7. Luminescence decay curves corresponding to the $^5D_0 \rightarrow {}^7F_2$ transition of Eu^{3+} ions in PCBGO and PCBGF glasses recorded at λ_{ex}= 394 nm and λ_{em}= 613 nm

radiative pathways. The reduced OH^- concentration previously identified in PCBGF glass likely contributes to its enhanced photoluminescence efficiency and stronger red emission intensity. It should be noted that the present study did not include measurement of thermal stability parameters (Tg, Tc) or absolute quantum yield, both of which are important for a complete evaluation of the material's suitability for solid-state laser applications. These parameters, together with the laser damage threshold, will be addressed in future work to further assess the practical applicability of this glass system.

Radiative Properties

The radiative characteristics of Eu^{3+} doped PCBGO and PCBGF glasses derived from the Judd-Ofelt analysis are summarized in TABLE 5. Several important spectroscopic parameters were evaluated, including peak emission wavelength (λ_p), effective bandwidth ($\Delta\lambda_{eff}$), stimulated emission cross-section ($\sigma_e(\lambda_p)$), branching ratio (β_R), radiative transition probability (A_R), and radiative lifetime (τ_R). These parameters are highly important for determining the suitability of luminescent materials for photonic applications such as solid-state lasers, optical amplifiers, phosphors, and light-emitting devices [37-38]. The observed radiative transitions originate from the excited $^5D_0$ level of Eu^{3+} ions toward the lower ^7F_J (J = 0-4) energy levels. The strongest emission band for both glasses occurs at 613 nm, corresponding to the hypersensitive $^5D_0 \rightarrow {}^7F_2$ transition. This transition exhibits the highest experimental branching ratio (β_R) and stimulated emission cross-section ($\sigma_e(\lambda_p)$) among all observed transitions, indicating that the red emission transition is the dominant radiative channel in both glass systems. The dominance of the $^5D_0 \rightarrow {}^7F_2$ transition further confirms the existence of non-centrosymmetric local environments surrounding Eu^{3+} ions within the silica-phosphate glass network [39].

The branching ratio β_R is an important parameter for evaluating the probability of radiative emission through a specific transition channel. Generally, transitions with β_R values exceeding 0.5 are considered highly favorable for laser and luminescent applications because they

TABLE 5. The radiative characteristics of PCBGO and PCBGF glass hosts, including peak emission wavelength (λ_p), effective bandwidth ($\Delta\lambda_{eff}$), emission cross section at peak ($\sigma_e(\lambda_p) \times 10^{-22}$ cm^2), branching ratio (β_R), and radiative transition probability (A_R).

Glass	Transition $^5D_0 \rightarrow$	λ_p (nm)	$\Delta\lambda_{eff}$ (nm)	$\sigma_e(\lambda_p)$ (cm^2)	β_{exp} (%)	β_{cal} (%)	A_R (s^{-1})	τ_R	
								J-O (ms)	Exp (ms)
PCBGO	$^7F_0$	578	6.91	0.00	0.0086	0	0.00	5.208	1.823
	$^7F_1$	591	21.74	1.53	0.2081	0.2468	47.40		
	$^7F_2$	613	23.53	1.67	0.7114	0.2836	54.46		
	$^7F_3$	653	12.09	0.00	0.0150	0	0.000		
	$^7F_4$	700	14.65	7.99	0.0570	0.4674	89.77		
PCBGF	$^7F_0$	578	5.15	0.00	0.0060	0	0.00	7.980	1.029
	$^7F_1$	591	20.91	1.70	0.2054	0.4089	51.24		
	$^7F_2$	613	20.98	1.93	0.7195	0.4161	52.15		
	$^7F_3$	653	10.94	0.00	0.0147	0.0000	0.000		
	$^7F_4$	700	12.82	2.23	0.0543	0.1701	21.32		

contribute significantly to the total radiative emission. As presented in TABLE 5, the $^5D_0 \rightarrow ^7F_2$ transition exhibits β_R values of 0.7114 for PCBGO and 0.7195 for PCBGF, which are considerably higher than those of other transitions. These results indicate that the red emission centered at 613 nm possesses the highest potential for stimulated emission and optical amplification. The large β_R values are also consistent with the strong photoluminescence intensity observed in the emission spectra. Another important parameter related to laser performance is the stimulated emission cross-section $\sigma_e(\lambda_p)$, which represents the ability of the material to generate stimulated emission. Higher $\sigma_e(\lambda_p)$ values generally correspond to lower laser threshold energy and higher optical gain [26]. For the $^5D_0 \rightarrow ^7F_2$ transition, PCBGF glass exhibits a higher stimulated emission cross-section value (1.93×10^{-22} cm^2) compared with PCBGO (1.67×10^{-22} cm^2). This enhancement suggests that the fluoride-containing glass provides a more favorable optical environment for stimulated emission processes. The improved $\sigma_e(\lambda_p)$ value in PCBGF can be attributed to reduced multi phonon relaxation and lower phonon energy induced by GdF_3 incorporation, which enhances radiative transition efficiency. The effective bandwidth $\Delta\lambda_{eff}$ also plays a crucial role in determining the amplification capability of optical materials. Broad emission bandwidths are advantageous for tunable laser and broadband optical amplifier applications. PCBGO glass exhibits a slightly broader effective bandwidth for the $^5D_0 \rightarrow ^7F_2$ transition (23.53 nm) compared with PCBGF (20.98 nm), indicating that the oxide-based glass possesses a broader spectral emission profile. However, despite the narrower bandwidth, PCBGF still demonstrates superior emission intensity and larger stimulated emission cross-section due to its enhanced radiative efficiency.

The radiative transition probability A_R describes the probability of spontaneous emission from an excited state to a lower energy level. Larger A_R values generally indicate stronger radiative transitions and more efficient luminescence behavior. In PCBGO glass, the highest A_R value is observed for the $^5D_0 \rightarrow ^7F_4$ transition (89.77 s^{-1}), whereas PCBGF exhibits its highest A_R value for the $^5D_0 \rightarrow ^7F_2$ transition (52.15 s^{-1}). These differences indicate that the local structural environment strongly affects the transition dynamics of Eu^{3+} ions. The fluoride-containing PCBGF glass promotes stronger electric-dipole transitions associated with the hypersensitive $^5D_0 \rightarrow ^7F_2$ emission, whereas the oxide-based PCBGO glass favors broader radiative distribution among multiple transitions. The calculated radiative lifetimes obtained from Judd-Ofelt analysis are 5.208 ms for PCBGO and 7.980 ms for PCBGF. The longer calculated radiative lifetime in PCBGF suggests lower non-radiative relaxation probability and improved optical efficiency within the fluoride-containing matrix. Such behavior is commonly observed in fluorinated glass systems because fluoride ions significantly reduce phonon-assisted energy losses [16, 37]. Therefore, the radiative properties confirm that GdF_3 incorporation effectively improves the optical performance and luminescent characteristics of Eu^{3+} doped silica-phosphate glasses.

CIE Chromaticity Diagram

The color characteristics of the emitted luminescence from Eu^{3+} doped PCBGO and PCBGF glasses were evaluated using the Commission Internationale de l'Éclairage (CIE) 1931

chromaticity diagram, as presented in FIGURE 8. The chromaticity coordinates were determined from the photoluminescence emission spectra by converting the emission intensity distribution into the standard CIE tristimulus color functions [40]. The obtained chromaticity coordinates for both PCBGO and PCBGF glasses were calculated to be (x = 0.571, y = 0.302). The identical coordinate values indicate that the substitution of Gd_2O_3 by GdF_3 does not significantly alter the dominant emission color of the Eu^{3+} ions. As illustrated in Figure 8, these coordinates are located within the red region of the CIE chromaticity diagram, confirming that both prepared glasses exhibit strong red luminescence. The observed red emission is primarily dominated by the hypersensitive $^5D_0 \rightarrow {}^7F_2$ transition of Eu^{3+} centered at approximately 613 nm, which was also identified as the strongest emission band in the photoluminescence spectra. The position of the chromaticity coordinates near the pure red region demonstrates the excellent color purity of the prepared glasses. Such behavior is highly desirable for applications requiring stable red emission, including red phosphors for white light-emitting diodes (WLEDs), optical display technologies, luminescent converters, and laser materials [26]. The strong red emission also confirms that Eu^{3+} ions occupy non-centrosymmetric local environments within the silica-phosphate glass network, resulting in enhanced electric-dipole transition probability for the $^5D_0 \rightarrow {}^7F_2$ transition.

Although both glasses exhibit identical chromaticity coordinates, the PCBGF sample showed higher photoluminescence intensity compared with PCBGO, indicating that fluoride incorporation enhances emission efficiency without changing the emission colour. This phenomenon suggests that the incorporation of GdF_3 mainly influences the radiative efficiency and local structural environment surrounding Eu^{3+} ions rather than altering the electronic transition mechanism responsible for red emission. The reduced phonon energy and lower hydroxyl concentration in PCBGF glass contribute to improved luminescence intensity while preserving the characteristic Eu^{3+} emission profile.

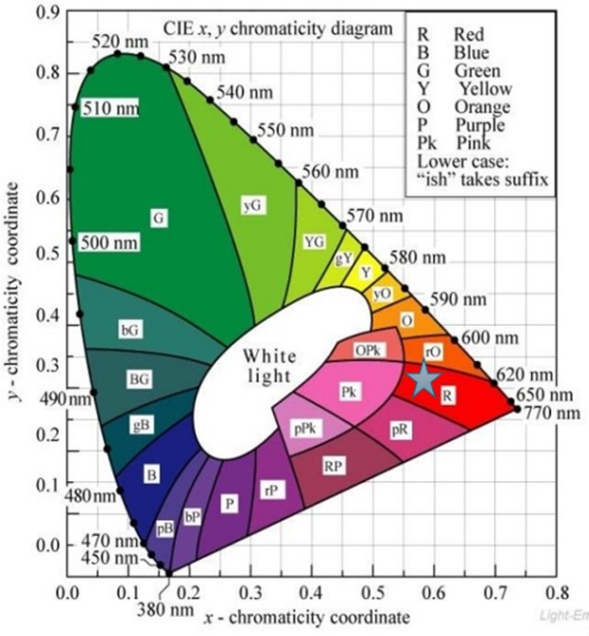

FIGURE 8. CIE-1931 chromaticity diagram of Eu^{3+} doped PCBGO and PCBGF silica-phosphate glasses.

CONCLUSION

Eu^{3+} doped gadolinium silica-phosphate glasses with compositions of $57P_2O_5$-15QS-15CaO-5BaO-$5Gd_2O_3$-$3Eu_2O_3$ (PCBGO) and $57P_2O_5$-15QS-15CaO-5BaO-$5GdF_3$-$3Eu_2O_3$ (PCBGF) were successfully fabricated using the melt-quenching technique employing Huta Ginjang quartz sand as a natural silica source. XRD analysis confirmed the amorphous nature of both glasses, while FTIR spectra verified the formation of silica-phosphate structural networks consisting of phosphate and silica vibrational units. The incorporation of GdF_3 significantly influenced the structural environment by reducing hydroxyl-related defects and producing a more open and transparent glass network compared with the oxide-based PCBGO glass. Optical absorption analysis revealed characteristic Eu^{3+} transitions in the UV-Vis-NIR regions, and Judd-Ofelt analysis demonstrated that PCBGF glass possessed higher Ω_2 values, indicating greater local asymmetry and stronger covalent interaction surrounding Eu^{3+} ions. Photoluminescence studies showed intense red emission dominated by the hypersensitive $^5D_0 \rightarrow {}^7F_2$ transition at 613 nm for both excitation wavelengths of 275 and 394 nm. PCBGF glass exhibited significantly enhanced excitation and emission intensities due to reduced phonon energy and improved radiative efficiency induced by fluoride incorporation. The stimulated emission cross-section and branching ratio values further confirmed the strong potential of the $^5D_0 \rightarrow {}^7F_2$ transition for photonic applications. Lifetime analysis revealed shorter decay time in PCBGF glass, indicating enhanced radiative transition probability and efficient luminescence processes. Moreover, the CIE chromaticity coordinates of both glasses were located in the pure red region, confirming their suitability as red-emitting photonic materials. Overall, the obtained results demonstrate that GdF_3 incorporation effectively enhances the optical and photoluminescence properties of Eu^{3+} doped silica-phosphate glasses, making PCBGF a promising candidate for red phosphors, optical amplifiers, solid-state lasers, and advanced photonic devices. However, this study is limited to structural and optical characterization based on indirect probes (XRD, FTIR, and Judd–Ofelt analysis) under laboratory conditions, without direct local structural confirmation (e.g., EXAFS, NMR) or measurement of thermal stability parameters (Tg, Tc) and absolute quantum yield. Future research should therefore focus on complementary structural characterization, thermal analysis, and absolute quantum yield measurements to further validate the proposed structural and relaxation mechanisms. In addition, fabrication of these glasses into practical device prototypes, such as optical fibers, waveguides, or thin films, along with evaluation of parameters such as laser damage threshold and gain characteristics, is recommended as a necessary step toward realizing their practical application in solid-state laser and LED devices.

ACKNOWLEDGEMENTS

This research was funded by the Ministry of Higher Education, Sciences, and Technology, Republic of Indonesia (Grant No. 245/C3/DT3.05.00/PL-BARU/2026). We are also grateful to The Center of Excellence in Glass Teachnology and Materials Sciences (**CEGM**), and Nakhon Pathom Rajabhat University for supporting this research.

REFERENCES

[1] J. Rocherullé et al., "Specific trends in phosphate glass crystallization," *J. Non-Cryst. Solids*, vol. 551, p. 120431, Jan. 2021, doi: 10.1016/j.jnoncrysol.2020.120431.

[2] R. K. Brow, "Review: the structure of simple phosphate glasses," *J. Non-Cryst. Solids*, vol. 263–264, pp. 1–28, Mar. 2000, doi: 10.1016/S0022-3093(99)00620-1.

[3] V. R. Teja, M. Sreenivasulu, and V. K. Chavan, "Glasses doped with europium ions for use in optoelectronic devices: W-LED," *Ceram. Int.*, vol. 51, no. 8, pp. 10077–10094, Mar. 2025, doi: 10.1016/j.ceramint.2024.12.439.

[4] B. Qian, X. Liang, C. Wang, and S. Yang, "Structure and properties of calcium iron phosphate glasses," *J. Nucl. Mater.*, vol. 443, no. 1–3, pp. 140–144, Nov. 2013, doi: 10.1016/j.jnucmat.2013.07.014.

[5] P. A. Bingham, R. J. Hand, O. M. Hannant, S. D. Forder, and S. H. Kilcoyne, "Effects of modifier additions on the thermal properties, chemical durability, oxidation state and structure of iron phosphate glasses," *J. Non-Cryst. Solids*, vol. 355, no. 28–30, pp. 1526–1538, Aug. 2009, doi: 10.1016/j.jnoncrysol.2009.03.008.

[6] N. Chanthima, J. Kaewkhao, Y. Tariwong, N. Sangwaranatee, and N. W. Sangwaranatee, "Luminescence study and Judd-Ofelt analysis of CaO-BaO-P2O5 glasses doped with Nd3+ ions," *Mater. Today Proc.*, vol. 4, no. 5, pp. 6091–6098, 2017, doi: 10.1016/j.matpr.2017.06.099.

[7] Z. S. Ngara, "Sintesis dan kajian sifat optik dan pola-pola difraksi sinar-X senyawa kompleks 1,10 phenanthroline," *Jurnal Fisika: Fisika Sains dan Aplikasinya*, vol. 7, no. 2, pp. 27–30, Oct. 2022, doi: 10.35508/fisa.v7i2.9342.

[8] D. S. Raju, S. H. Bindu, J. S. Krishna, V. V. Krishna, and C. L. Raju, "Synthesis and structural analysis of trivalent europium (Eu3+) ions doped oxyfluoride (ZnBiNaPSr) glasses as prominent host materials for optical devices," *J. Phys. Conf. Ser.*, vol. 1913, no. 1, p. 012011, May 2021, doi: 10.1088/1742-6596/1913/1/012011.

[9] J. Rajagukguk et al., "Radioluminescence properties of huta ginjang quartz sand doped with CeF3 and Tb2O3 for scintillator application," *Radiat. Phys. Chem.*, vol. 223, p. 111939, Oct. 2024, doi: 10.1016/j.radphyschem.2024.111939.

[10] R. Ahlawat, N. Rani, and B. Goswami, "Synthesis and characterizations of Eu2O3 nanocrystallites and its effect on optical investigations of Eu3+, Eu2+: SiO2 nanopowder," *J. Alloys Compd.*, vol. 743, pp. 126–135, 2018, doi: 10.1016/j.jallcom.2018.01.360.

[11] N. Wantana, S. Kaewjaeng, S. Kothan, H. J. Kim, and J. Kaewkhao, "Energy transfer from Gd3+ to Sm3+ and luminescence characteristics of CaO–Gd2O3–SiO2–B2O3 scintillating glasses," *J. Lumin.*, vol. 181, pp. 382–386, 2017, doi: 10.1016/j.jlumin.2016.09.050.

[12] C. Li et al., "Physical and optical properties of TeO2-WO3-GdF3 tellurite glass system," *Ceram. Int.*, vol. 48, no. 9, pp. 12497–12505, May 2022, doi: 10.1016/j.ceramint.2022.01.116.

[13] L. Fu, Y. Wu, C. Zhang, T. Fu, and C. Shi, "Determination of radiative and multiphonon non-radiative relaxation rates of upconversion materials," *Phys. Chem. Chem. Phys.*, vol. 24, no. 17, pp. 9953–9963, 2022, doi: 10.1039/D2CP00978A.

[14] J. Rajagukguk, J. H. Panggabean, M. Djamal, C. S. Sarumaha, and J. Kaewkhao, "Energy transfer and broad-band luminescence of Nd3+-Er3+ co-doped lithium fluorophosphate (LFP) glasses," *Opt. Mater.*, vol. 125, p. 112007, Mar. 2022, doi: 10.1016/j.optmat.2022.112007.

[15] M. Poulain, "Heavy metal fluoride glasses: a tutorial review," *APL Photonics*, vol. 9, no. 9, Sep. 2024, doi: 10.1063/5.0226668.

[16] S. M. K. Gedara, Z.-Y. Ding, I. L. Balasooriya, Y. Han, and M. N. Wickramaratne, "Hydrothermal synthesis and in vivo fluorescent bioimaging application of Eu3+/Gd3+ co-doped fluoroapatite nanocrystals," *J. Funct. Biomater.*, vol. 13, no. 3, p. 108, Jul. 2022, doi: 10.3390/jfb13030108.

[17] Z. Wang, Z. Liu, W. Wang, Z. M. Shi, N. Pang, and C. Wang, "Effect of desert-sand replacing pure SiO2 on crystallization, densification and properties of cordierite glass-ceramic," *J. Mater. Res. Technol.*, vol. 31, pp. 2202–2216, Jul. 2024, doi: 10.1016/j.jmrt.2024.07.001.

[18] J. H. Panggabean, J. Rajagukguk, D. Rajagukguk, C. Sarumaha, and J. Kaewkhao, "The effect of calcium fluoride in lithium phosphate oxide (LPO) doped with Sm3+ content," *Integr. Ferroelectr.*, vol. 224, no. 1, pp. 110–119, 2022, doi: 10.1080/10584587.2022.2035601.
[19] E. M. Abou Hussein and A. Sobhy, "Experimental investigation of new rare earth borosilicate glasses from municipal waste ash as high-dose radiation dosimeters," *Ceram. Int.*, vol. 50, no. 13, pp. 23012–23024, Jul. 2024, doi: 10.1016/j.ceramint.2024.04.023.
[20] M. Shoaib et al., "Effect of Gd2O3 and GdF3 on physical and luminescence properties of Ce3+ ion-doped phosphate glasses: a comparative study," *Braz. J. Phys.*, vol. 55, no. 5, p. 194, Oct. 2025, doi: 10.1007/s13538-025-01824-8.
[21] J. Rajagukguk, Fitrilawati, B. Sinaga, and J. Kaewkhao, "Structural and spectroscopic properties of Er3+ doped sodium lithium borate glasses," *Spectrochim. Acta A Mol. Biomol. Spectrosc.*, vol. 223, p. 117342, 2019, doi: 10.1016/j.saa.2019.117342.
[22] J. Rajagukguk et al., "Structural, spectroscopic and optical gain of Nd3+ doped fluorophosphate glasses for solid state laser application," *J. Lumin.*, vol. 216, p. 116738, Dec. 2019, doi: 10.1016/j.jlumin.2019.116738.
[23] H. Fneich, N. Gaumer, S. Chaussedent, W. Blanc, and A. Mehdi, "Europium-doped sol-gel SiO2-based glasses: effect of the europium source and content, magnesium addition and thermal treatment on their photoluminescence properties," *Molecules*, vol. 23, no. 7, pp. 1–14, 2018, doi: 10.3390/molecules23071768.
[24] N. A. S. Omar, Y. W. Fen, K. A. Matori, S. H. A. Aziz, Z. N. Alassan, and N. F. Samsudin, "Development and characterization studies of Eu3+-doped Zn2SiO4 phosphors with waste silicate sources," *Procedia Chem.*, vol. 19, pp. 21–29, 2016, doi: 10.1016/j.proche.2016.03.006.
[25] S. Yin et al., "Study on the optical properties of high refractive index TeO2-PbO-ZnO-BaF2 glass system," *Adv. Mater. Sci. Eng.*, vol. 2021, no. 1, Jan. 2021, doi: 10.1155/2021/6466344.
[26] N. Wantana et al., "High density tungsten gadolinium borate glasses doped with Eu3+ ion for photonic and scintillator applications," *Radiat. Phys. Chem.*, vol. 172, p. 108868, Jul. 2020, doi: 10.1016/j.radphyschem.2020.108868.
[27] D. H. Rajagukguk, J. Rajagukguk, R. Juliani, C. Sarumaha, and J. Kaewkhao, "Influence of calcium fluoride on the radiative properties of Sm3+ doped zinc borophosphate glasses," *Integr. Ferroelectr.*, vol. 239, no. 1, pp. 183–196, Nov. 2023, doi: 10.1080/10584587.2023.2234621.
[28] V. Ravi Teja, M. Sreenivasulu, and V. K. Chavan, "Optical applications of europium ion doped silicate glasses: W-LED," *Silicon*, vol. 16, no. 8, pp. 3553–3571, Jun. 2024, doi: 10.1007/s12633-024-02942-9.
[29] S. Bebars, A. S. Gadallah, M. A. Khedr, and M. T. H. Abou Kana, "Judd-Ofelt and laser parameters of Eu3+ ions doped in network restricted matrices," *J. Lumin.*, vol. 192, pp. 949–956, Aug. 2017, doi: 10.1016/j.jlumin.2017.08.025.
[30] G.-J. Shu et al., "Unraveling the electronic structures in different phases of gadolinium sesquioxides performed by electron energy loss spectroscopy," *AIP Adv.*, vol. 10, no. 10, Oct. 2020, doi: 10.1063/5.0025978.
[31] J. Rajagukguk, J. Kaewkhao, M. Djamal, R. Hidayat, Suprijadi, and Y. Ruangtaweep, "Structural and optical characteristics of Eu3+ ions in sodium-lead-zinc-lithium-borate glass system," *J. Mol. Struct.*, vol. 1121, pp. 180–187, 2016, doi: 10.1016/j.molstruc.2016.05.048.
[32] C. S. Sarumaha et al., "Effect of Gd2O3 in Li2O–AlF3–CaF2–P2O5–Eu2O3 glasses for laser medium and X-rays detection material applications," *Radiat. Phys. Chem.*, vol. 199, p. 110362, Oct. 2022, doi: 10.1016/j.radphyschem.2022.110362.
[33] A. Abdallah and C. Bouzidi, "Optical characterization of Eu3+/Gd3+ co-doped phosphate glasses for efficient energy transfer," *Opt. Mater.*, vol. 172, p. 117819, Apr. 2026, doi: 10.1016/j.optmat.2025.117819.
[34] S. Oğuzlar, M. Zeyrek Ongun, and A. M. Deliormanlı, "Modulation of optical oxygen sensitivity of H2(TPP) by using Eu3+, Gd3+ and Yb3+ ions doped silicate-based bioactive glass powders immersed in simulated body fluid," *Optik*, vol. 294, p. 171458, Dec. 2023, doi: 10.1016/j.ijleo.2023.171458.

[35] R. Rajaramakrishna, P. Nijapai, P. Kidkhunthod, H. J. Kim, J. Kaewkhao, and Y. Ruangtaweep, "Molecular dynamics simulation and luminescence properties of Eu3+ doped molybdenum gadolinium borate glasses for red emission," *J. Alloys Compd.*, vol. 813, p. 151914, Jan. 2020, doi: 10.1016/j.jallcom.2019.151914.

[36] M. Shoaib et al., "Photoluminescence analysis of Er3+-ions doped P2O5-Gd2O3/GdF3-BaO-ZnO glass systems," *J. Alloys Compd.*, vol. 902, p. 163766, May 2022, doi: 10.1016/j.jallcom.2022.163766.

[37] V. L. Usharani and B. Eraiah, "Synthesis, structural and luminescence studies of europium doped borate glasses," *J. Mater. Appl.*, vol. 9, no. 1, pp. 9–16, May 2020, doi: 10.32732/jma.2020.9.1.9.

[38] J. Rajagukguk et al., "Radio and photo luminescence of Dy3+ doped lithium fluorophosphate scintillating glass," *Radiat. Phys. Chem.*, vol. 185, Aug. 2021, doi: 10.1016/j.radphyschem.2021.109520.

[39] Z. Zou, S. Yang, and Y. Li, "Enhanced luminescence performance of BaY4Si5O17:Eu3+, Gd3+ red phosphors via energy transfer for WLED applications," *Ceram. Int.*, vol. 51, no. 22, pp. 37652–37660, Sep. 2025, doi: 10.1016/j.ceramint.2025.06.016.

[40] D. A. Rodríguez-Carvajal, A. N. Meza-Rocha, U. Caldiño, R. Lozada-Morales, E. Álvarez, and Ma. E. Zayas, "Reddish-orange, neutral and warm white emissions in Eu3+, Dy3+ and Dy3+/Eu3+ doped CdO-GeO2-TeO2 glasses," *Solid State Sci.*, vol. 61, pp. 70–76, Nov. 2016, doi: 10.1016/j.solidstatesciences.2016.09.009.